Optical-parametric-generation process driven by femtosecond pulses: Timing and carrier-envelope phase properties

C. Manzoni,* G. Cirmi, D. Brida, S. De Silvestri, and G. Cerullo
Dipartimento di Fisica, National Laboratory for Ultrafast and Ultraintense Optical Science-INFM-CNR, Politecnico di Milano, Piazza L. Da Vinci 32, 20133 Milano, Italy
(Received 19 November 2008; published 16 March 2009)

We investigate, both numerically and experimentally, the optical parametric generation (OPG) process in second-order nonlinear crystals driven by femtosecond pulses. We model the OPG process by solving the coupled second-order three-wave nonlinear propagation equations in the plane-wave limit, using noise fields to mimic the vacuum fluctuations. We focus on two parameters: (i) the temporal jitter between the OPG and the pump pulse; (ii) the carrier-envelope phase (CEP) relationship between the OPG and the pump pulse. Both numerical simulations and experiments support the following conclusions: (i) in the regime of low pump depletion the OPG pulse is synchronized with the pump, but its energy presents strong fluctuations; (ii) in the regime of high pump depletion, the energy of the OPG pulse stabilizes, but a temporal jitter with respect to the pump pulse is introduced; (iii) in both cases, the CEP relationship between pump and OPG pulses is completely random.

DOI: 10.1103/PhysRevA.79.033818 PACS number(s): 42.65.Re, 42.65.Yj, 42.65.Lm

I. INTRODUCTION

Many studies of nonlinear light-matter interaction require ultrashort light pulses with broadly tunable carrier wavelength [1]. Optical parametric amplifiers (OPAs) [2] are powerful instruments to achieve such tunability. In an OPA an high frequency and high intensity beam (the pump beam, at frequency ω_3) amplifies, in a suitable second-order nonlinear crystal, a lower frequency, lower intensity beam (the signal beam, at frequency ω_1); in addition a third beam (the idler beam, at frequency ω_2, with $\omega_1 < \omega_2 < \omega_3$) is generated. In the interaction, energy conservation $\hbar\omega_3 = \hbar\omega_1 + \hbar\omega_2$ is satisfied; for efficient energy transfer, also the momentum conservation (or phase matching) condition $\hbar\mathbf{k_3} = \hbar\mathbf{k_1} + \hbar\mathbf{k_2}$ must be fulfilled. OPAs driven by femtosecond lasers are nowadays workhorses in many nonlinear optics laboratories.

The first stage of any OPA system is the generation of the initial signal pulse to be amplified, the so-called "seed" pulse. Since the seed is at a different frequency from the pump, it must be generated by a nonlinear optical process. The seed pulse of an OPA is usually produced by two means: white-light continuum (WLC) generation [3] and parametric superfluorescence [4], also known as optical parametric generation (OPG). WLC generation is a third-order nonlinear process occurring when a femtosecond pulse is tightly focused in a transparent medium [5] (typically a sapphire plate) resulting in a combination of temporal self-phase-modulation (SPM), spatial self-focusing, and other linear and nonlinear optical processes [6], leading to the formation of a spatial filament and to a dramatic spectral broadening. OPG is parametric amplification of the vacuum or quantum noise and can also be thought as two-photon spontaneous emission from a virtual level excited by the pump field [7]. In practice it is simply achieved by pumping a suitable nonlinear crystal, which is often of the same type as the ones used in the subsequent OPA stages; amplification will occur at those wavelengths for which the parametric interaction is phase matched [8,9]. WLC presents several advantages as a seed such as higher pulse-to-pulse stability and superior spatial beam quality; on the other hand, it poses rather tight requirements on the characteristics of the driving pulse such as energy higher than 1–2 μJ and pulse width shorter than 200–250 fs [10]. Such parameters are not always easy to achieve, in particular for lasers systems (such as ytterbium-based bulk and fiber lasers) producing moderate energy pulses (a few μJs) at high repetition rates (up to a few megahertz). For such systems the OPG approach is practically more attractive, especially using crystals with very high effective nonlinearity (such as periodically poled lithium niobate and lithium tantalate) that allow achieving large parametric gains with relatively low pump energies. In addition, in some instances the parametric gain is so large that the OPG process by itself can be used for efficient frequency conversion without additional OPA stages [11–17]. Apart from conversion efficiency, other parameters should be considered to determine if OPG is a good source of femtosecond pulses. In particular many applications employing ultrashort laser pulses, such as time-resolved spectroscopy and nonlinear optics, strongly require high pulse-to-pulse energy stability and an accurate synchronization of two independent sources. Therefore, a full understanding of the OPG process with femtosecond driving pulses calls for an accurate analysis of the energy fluctuations and timing jitter of the generated pulses.

OPAs can also be used for the generation of pulses with controlled carrier-envelope phase (CEP) ϕ, enabling the synthesis of optical waveforms with reproducible electric field profile [18]. Such control is important for pulses with few-optical-cycle duration, for which a CEP variation produces a strong change in the waveform. In this case and at high-intensity interactions, the so-called extreme nonlinear optics regime, it is possible to observe CEP-dependent phenomena such as above-threshold ionization [19] and high-order har-

*Corresponding author. cristian.manzoni@polimi.it

monic generation (HHG) [20]. In particular, CEP control is a prerequisite for the production of isolated attosecond pulses through HHG [21,22]. Mode-locked laser oscillators emit pulse trains in which the CEP changes from one pulse to the other due to the difference between phase and group velocity in the materials constituting the laser cavity [23]. CEP stabilization can be achieved using either active or passive methods. Passive schemes, pioneered by Baltuška *et al.* [24], rely on difference frequency generation (DFG) between two pulses sharing the same CEP: in this process the phases of the two pulses add up with opposite signs leading to automatic cancellation of the pulse-to-pulse CEP fluctuations. Passive CEP stabilization has the advantages of being an all-optical technique, without any electronic feedback circuitry, and of allowing the generation of pulses tunable in a broad frequency range. In an OPA the idler pulse arises from the DFG between pump and signal pulses [25]: if pump and seed are CEP-locked, then the idler pulses are CEP-stabilized [24]. For the generation of CEP-stable pulses from an OPA, therefore, CEP coherence between pump and seed becomes of crucial importance.

Several studies have shown that WLC generation in a bulk material preserves the CEP of the driving pulse; in particular Bellini and Hänsch [26] demonstrated stable spatial interference fringes between two WLCs produced by the same pulse, while Baum *et al.* [27] observed CEP locking between WLC-seeded OPAs both at the same and at different [28] frequencies. The physical reason for this CEP preservation is that the SPM induced by the pump pulse can be seen as a four-wave-mixing process [24], of the kind $\omega_4=\omega_1+\omega_2-\omega_3$, where ω_1, ω_2, and ω_3 are frequencies falling within the pump spectrum and ω_4 is the newly generated frequency. In this case the CEP relationship between the interacting frequencies is given by $\phi_4=\phi_1+\phi_2-\phi_3+\pi/2$. Since ω_1, ω_2, and ω_3 share the same CEP, being all components of the driving pulse, the new frequencies will track (apart from a constant factor) the CEP of the pump. Several CEP-stable OPA designs using a seed generated via SPM have been reported [29–31]. The phase preserving properties of the WLC process are also exploited in CEP measurements with the so-called f-to-$2f$ interferometer, which makes use of WLC and SPM to generate octave-spanning spectra [32].

Much less attention has been given to the study of the CEP properties during the OPG process; since OPG is initiated by vacuum fluctuations or quantum noise, one would expect that the CEP link between the pump and the OPG pulses is weak or completely lost. However, in a recent paper Hauri *et al.* [33] reported CEP stabilization of the idler of an OPG-seeded OPA, implying that the OPG process preserves the CEP of the pump pulse. This result calls for a comprehensive theoretical and experimental study of the CEP-preserving properties of the OPG process, which is currently lacking.

In this paper we present a numerical and experimental study of the OPG process driven by femtosecond pulses. By numerical modeling the OPG process in the plane-wave limit, we obtain the following conclusions: (i) in the regime of low pump depletion, the OPG pulse is synchronized to the pump, but its energy presents strong fluctuations; (ii) in the regime of high pump depletion, the energy of the OPG pulse stabilizes, but a temporal jitter with respect to the pump pulse is introduced; (iii) in both cases, the CEP relationship between pump and OPG pulses is completely random. Experimental results for an OPG based on β-barium borate (BBO) and driven by 50-fs pulses from an amplified Ti:sapphire laser fully confirm the predictions. Our results have important implications for (a) high-gain OPGs working in the pump-depletion regime, since the generated pulses display a time jitter with respect to the driving ones which may be relevant for time-resolved experiments; (b) the generation of CEP-stable pulses from OPAs, since they show that the idler self-phase-stabilization mechanism works only with a WLC seed.

The paper is organized as follows: in Sec. II we describe the numerical approach used to model the OPG process; in Sec. III we summarize the main results of the simulations; in Sec. IV we describe the experimental approach used to characterize the temporal jitter and CEP of the OPG pulses and present the results. Finally, in Sec. V we draw some brief conclusions.

II. MATHEMATICAL FORMULATION

The OPG process is an intrinsically quantum-mechanical phenomenon. Since the 1960s it has been described mainly by two methods: a full quantum-mechanical treatment [34] and a two-stage semiclassical approach based on nonlinear interaction of classical fields with a quantum-mechanical initiation mimicked by a noise field [35,36]. The two approaches have been demonstrated to be equivalent [37]. In this paper we describe the OPG process by coupled nonlinear wave equations initiated by a noise field. An ultrabroadband noise field seeding both the signal and the idler beams acts as the quantum-mechanical source of parametric generation; the subsequent propagation and interaction of these fields with the strong driving pump field is then described by the classical nonlinear equations accounting for optical parametric amplification.

Let us first consider the equations describing the second-order nonlinear interactions among signal, idler, and pump fields, which in the following will be, respectively, labeled $i=1,2,3$. These waves propagate with carrier frequency ω_i and wave number k_i, and experience a phase-mismatch $\Delta k=k_3-k_2-k_1$. A complete description of the OPG process would require a three-dimensional model accounting for the transverse structure of the beams; nevertheless, a one-dimensional (1D) plane-wave model allows investigating the fluctuations in signal intensity, energy, and spectrum with sufficient accuracy [35]. Previous works considering also transverse effects showed that any off-axis parametric mode exhibits the same statistical behavior as the on-axis one [38]. In addition the purpose of the present work is the analysis of the properties of collinear superfluorescence only, which in practical applications can be easily selected by means of a spatial filter. For these reasons we focused on a 1D model and developed the equations needed for a plane-wave approach. In this case we describe the electric field of each wave by [39]

$$E_i(z,t) = \tfrac{1}{2}\{A_i(z,t)\exp[j(\omega_i t - k_i z)] + \text{c.c.}\} = \text{Re}\{A_i(z,t)\exp[j(\omega_i t - k_i z)]\}, \quad (1)$$

where $A_i(z,t)$ denotes the field complex amplitude. The

coupled equations describing the second-order interaction of the fields are derived from the nonlinear propagation equation

$$\frac{\partial^2 E}{\partial z^2} - \mu_0 \frac{\partial^2 D_{\mathrm{L}}}{\partial t^2} = \mu_0 \frac{\partial^2 P_{\mathrm{NL}}}{\partial t^2} \tag{2}$$

applied on the total field $E(z,t)=E_1(z,t)+E_2(z,t)+E_3(z,t)$. Here $D_{\mathrm{L}}(z,t)=\varepsilon_0 \int \varepsilon_r(\tau) E(z,t-\tau) d\tau$ is the linear electric induction field accounting for the linear dispersion of the medium [40], and $P_{\mathrm{NL}}=2\varepsilon_0 d_{\mathrm{eff}} E(z,t)^2$ is the nonlinear polarization, where d_{eff} is the effective second-order nonlinear coefficient. Since in our model the process is triggered by a broadband noise field, and our purpose is to calculate the evolution of the OPG pulse with the highest accuracy, we avoid the slowly-varying-envelope approximation [3] typically adopted to simplify the calculations and consider the linear dispersion of the material to all orders [41]. For this purpose, we develop Eq. (2) in the frequency domain by taking its Fourier transform and obtaining

$$\frac{\partial^2 \tilde{E}}{\partial z^2} + \frac{\Omega^2 n(\Omega)^2}{c_0^2} \tilde{E} = -\mu_0 \Omega^2 \tilde{P}_{\mathrm{NL}}, \tag{3}$$

where $\tilde{E}(z,\Omega)=\mathcal{F}\{E(z,t)\}$ and $\tilde{P}_{\mathrm{NL}}(z,\Omega)=\mathcal{F}\{P_{\mathrm{NL}}(z,t)\}$ are the nonunitary Fourier transforms of the electric field and of the nonlinear polarization, respectively, Ω is the angular frequency and $n(\Omega)$ is the frequency-dependent refractive index. P_{NL} is developed rejecting components at frequencies different from ω_1, ω_2, and ω_3; when the fields E_i are not spectrally overlapped, it is possible to split Eq. (3) into three coupled equations which separately describe the evolution of the fields envelopes:

$$\begin{aligned}
&\frac{\partial^2 \tilde{A}_1}{\partial z^2} - j2k_1 \frac{\partial \tilde{A}_1}{\partial z} + b_1^2 \tilde{A}_1 = -c_1 e^{-j\Delta k z},\\
&\frac{\partial^2 \tilde{A}_2}{\partial z^2} - j2k_2 \frac{\partial \tilde{A}_2}{\partial z} + b_2^2 \tilde{A}_2 = -c_2 e^{-j\Delta k z},\\
&\frac{\partial^2 \tilde{A}_3}{\partial z^2} - j2k_3 \frac{\partial \tilde{A}_3}{\partial z} + b_3^2 \tilde{A}_3 = -c_3 e^{+j\Delta k z}.
\end{aligned} \tag{4}$$

In this case $\tilde{A}_i(z,\omega)=\mathcal{F}\{A_i(z,t)\}$ is the Fourier transform of the envelope amplitude of each field and $\omega=\Omega-\omega_i$ is the detuning from the carrier frequency ω_i; coefficients b_i^2 and c_i are defined as

$$b_i^2 = -k_i^2 + \tilde{k}_i^2, \quad \text{with } \tilde{k}_i = \frac{(\omega+\omega_i) n_i(\omega+\omega_i)}{c_0} \tag{5a}$$

and

$$c_1 = \left(\frac{\omega+\omega_1}{c_0}\right)^2 d_{\mathrm{eff}} \mathcal{F}\{A_3 A_2^*\}, \tag{5b}$$

$$c_2 = \left(\frac{\omega+\omega_2}{c_0}\right)^2 d_{\mathrm{eff}} \mathcal{F}\{A_3 A_1^*\}, \quad c_3 = \left(\frac{\omega+\omega_3}{c_0}\right)^2 d_{\mathrm{eff}} \mathcal{F}\{A_1 A_2\}.$$

Here $n_i(\omega+\omega_i)$ are the refractive index functions deduced from Sellmeier's equations, and allow to take into account the whole linear dispersion of the material. The system can be solved by applying the split-step method [42]: if a suitably small step Δz is chosen, the products $A_3 A_2^*$, $A_3 A_1^*$, and $A_1 A_2$ are nearly constant, and Eq. (4) can be solved analytically. Given the fields $\tilde{A}_i(z,\omega)$ at the beginning of a step, the fields at $z+\Delta z$ are

$$\begin{aligned}
\tilde{A}_1(z+\Delta z,\omega) &\approx \left[\tilde{A}_1(z,\omega) + \frac{c_1}{\gamma_1}\right] \exp[j(k_1-\tilde{k}_1)\Delta z] - \frac{c_1}{\gamma_1} \exp[-j\Delta k \Delta z],\\
\tilde{A}_2(z+\Delta z,\omega) &\approx \left[\tilde{A}_2(z,\omega) + \frac{c_2}{\gamma_2}\right] \exp[j(k_2-\tilde{k}_2)\Delta z] - \frac{c_2}{\gamma_2} \exp[-j\Delta k \Delta z],\\
\tilde{A}_3(z+\Delta z,\omega) &\approx \left[\tilde{A}_3(z,\omega) + \frac{c_3}{\gamma_3}\right] \exp[j(k_3-\tilde{k}_3)\Delta z] - \frac{c_3}{\gamma_3} \exp[+j\Delta k \Delta z],
\end{aligned} \tag{6}$$

where $\gamma_{1,2}=b_{1,2}^2-\Delta k^2-2k_{1,2}\Delta k$ and $\gamma_3=b_3^2-\Delta k^2+2k_3\Delta k$. Note that when $d_{\mathrm{eff}}=0$, corresponding to absence of nonlinear interactions, $c_i=0$ and Eq. (6) give the typical solutions for linear propagation.

Let us now focus on the random electric fields introduced to mimic the quantum-mechanical superfluorescence generation process. Such fields arise from zero-point fluctuation of the vacuum and seed both signal and idler. In this paper we describe them by noise waves $A_\eta(\omega)$ in the frequency domain with the following form:

$$A_\eta(\omega) = \eta(\omega) e^{j\varphi(\omega)}, \tag{7}$$

where $\eta(\omega)$ is a Gaussian stochastic variable [35,36] with zero mean and variance σ^2 proportional to the field intensity, whereas $\varphi(\omega)$ has a uniform distribution from $-\pi$ to $+\pi$. Both variables are uncorrelated with each other; in addition their spectral correlation is given by

$$\langle \eta(\omega) \eta^*(\omega') \rangle = \sigma^2 \delta(\omega-\omega') \tag{8}$$

and

$$\langle \varphi(\omega) \varphi^*(\omega') \rangle = (\pi^2/3) \delta(\omega-\omega'). \tag{9}$$

This is actually not the only model proposed for the analytical description of the noise waves; other approaches can be adopted [38,43], the only differences being the statistical distributions of η and φ. However preliminary simulations that we conducted showed that different models give comparable results. The signal and idler beams $A_\eta(\omega)$ are randomly generated at the beginning of the crystal and act, together with

the pump, as boundary conditions for Eq. (6). To give a full statistical treatment of the OPG process, we conducted a set of 1000 independent simulations triggered by different noise fields; we expect that averages taken over such an ensemble of classical solutions do correspond to quantum-mechanical expectation values [44].

III. NUMERICAL SIMULATIONS AND RESULTS

For the OPG simulations we chose a BBO crystal pumped at 800 nm wavelength, close to our experimental conditions. We selected a type II (signal ordinary, idler extraordinary, pump extraordinary) phase-matching configuration, which is particularly suited for the generation of coherent transform-limited (TL) pulses in the femtosecond regime [14,45] thanks to the favorable group velocity mismatch (GVM) values. The main factor governing parametric interaction with ultrashort pulses is the GVM between the interacting pulses, expressed by the parameters $\delta_{31}=1/v_{g1}-1/v_{g3}$ and $\delta_{32}=1/v_{g2}-1/v_{g3}$, where v_{g1}, v_{g2}, and v_{g3} are the group velocities of signal, idler, and pump, respectively. Given a pump pulse with duration τ, one can define pulse splitting length as the propagation length after which the signal (or the idler) pulse temporally separates from the pump pulse in the absence of gain: $l_{31,2}=\tau\delta_{31,2}$. There is a qualitatively important difference between the cases in which δ_{31} and δ_{32} have the same or different signs. When $\delta_{31}\delta_{32}>0$, both the signal and the idler pulses walk away from the pump in the same direction, so that the gain rapidly decreases for propagation distances longer than the pulse splitting length and eventually saturates, preventing an efficient OPG process. On the other hand, when $\delta_{31}\delta_{32}<0$ signal and idler pulses walk in opposite direction with respect to the pump; in this way a nonlinear interaction mechanism localizes them under the pump pulse and the gain grows exponentially even for crystal lengths well in excess of the pulse splitting length. To qualitatively understand this trapping effect, we can consider the situation in which the signal pulse has moved slightly to the front and the idler pulse to the back of the pump pulse: during the parametric process, the signal pulse generates idler photons, which move to the back, i.e., toward the peak of the pump; on the other hand the idler pulse generates signal photons which in turn move to the front, again toward the peak of the pump. This effect, which takes place in all parametric amplification processes, is particularly useful in enhancing the OPG process: under these conditions, in fact, signal and idler photons are trapped under the pump pulse, and they can be amplified from the noise level to saturation, occurring at pump depletion. This effect becomes particularly relevant when the pump pulses have duration of tens of femtoseconds, as studied in this paper.

In our case, we considered a BBO crystal cut for phase matching of an ordinary polarized signal at 1.3 μm wavelength ($\theta=26°$); under these conditions, we have $\delta_{32}=-46.5$ fs/mm and $\delta_{31}=+23.5$ fs/mm, so that $\delta_{31}\delta_{32}<0$. Pump pulses have full width at half maximum (FWHM) duration of 50 fs, energy of 30 μJ, and spot size $w_0=0.3$ mm, which correspond, considering also Fresnel losses at the entrance surface of the crystal, to a peak intensity of

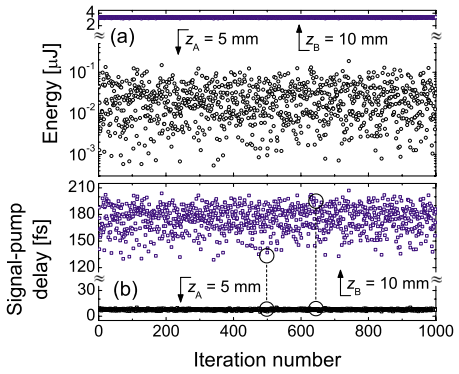

FIG. 1. (Color online) (a) Logarithmic scale: pulse energy of the signal beam obtained from a run of 1000 simulations of the parametric generation process before ($z_A=5$ mm) and after ($z_B=10$ mm) gain saturation. (b) Linear scale: delay of the OPG signal pulse with respect to the pump in z_A and z_B. For both panels, the scales are the same before and after the breaks, for ease of comparison; mean and standard deviation values of pulse energy and delay are given in Table I.

400 GW/cm^2; the pump CEP at $z=0$ is set to $\phi_p=0$. The random variables $\eta(\omega)$ and $\varphi(\omega)$ are generated by the modified subtract-with-borrow algorithm [46]; for each frequency, the variance of the noise field emitted collinearly to the pump is

$$\sigma^2 \approx Z_n\omega \tag{10}$$

according to the model proposed in Ref. [47] for the 1D case. Here Z_n is a parameter that we experimentally obtained from measurements on superfluorescence threshold in BBO. With these boundary conditions, preliminary simulations showed that amplification of the vacuum noise becomes significant for interaction lengths of about 3 mm and saturation is reached for crystal lengths of about 8 mm; to get an insight into the OPG process below and above gain saturation, we considered a crystal with thickness of 10 mm and we studied the signal field properties at crystal depths $z_A=5$ mm and $z_B=10$ mm, respectively, before and after saturation.

Figure 1 displays the energy of the signal pulse [panel (a)] and its time delay with respect to the pump pulse [panel (b)], monitored in z_A and z_B. As expected, since the OPG process starts at a random position inside the crystal, the energy exhibits very strong fluctuations below saturation (z_A) and gains stability only when pump depletion takes place (z_B). This confirms the well-known result that the OPG process can provide a stable energy only if driven into saturation [11–14]. On the other hand the pulse-to-pulse time jitter of the OPG pulse with respect to the pump has a radically different behavior, as shown in Fig. 1(b). Before saturation, the signal is nearly perfectly synchronized with the pump, as expected from the trapping effect occurring in type II parametric amplification. When the OPG process reaches saturation, this nonlinear effect vanishes, and signal and idler pulses experience linear propagation, walking in opposite directions with respect to the pump. This effect is clearly shown in Fig. 2, where we represent the temporal evolution of signal and idler pulses during their interaction along the

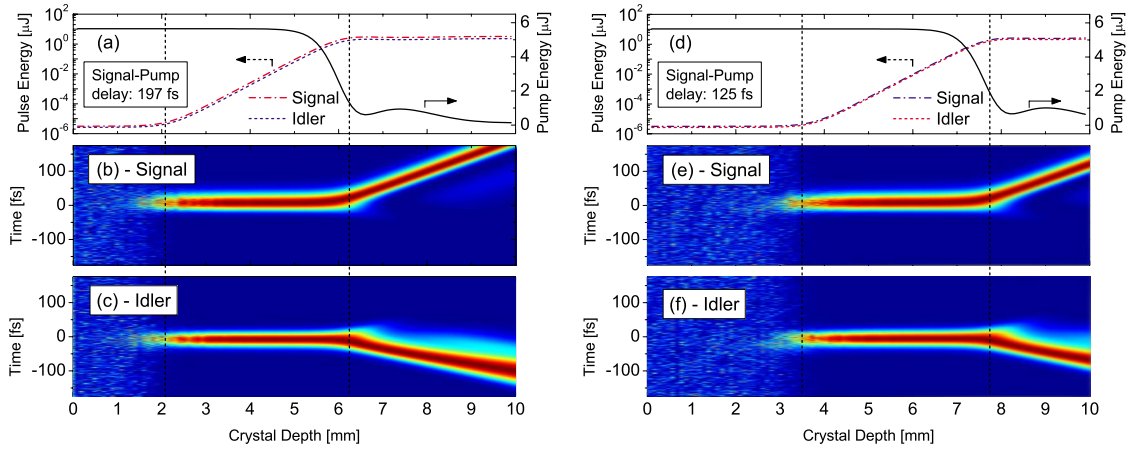

FIG. 2. (Color online) Temporal evolution of intensity-normalized signal and idler fields along the crystal, in a frame of reference moving with the pump; situations (a-b-c) and (d-e-f) differ only for the random noise fields initiating the OPG process and correspond to the two output signal-pump delays marked in Fig. 1(b). Panels (a) and (d) give the energy of the beams; the starting points of amplification and saturation regimes are also highlighted.

crystal, in a temporal frame of reference moving with the pump. The 2D maps trace the evolution of the normalized signal and idler fields along the crystal, from the fluctuating random fields to the saturated propagation. The figure clearly marks the differences between situations (a)–(c) and (d)–(f), driven by two different noise fields and corresponding to the two highlighted cases of Fig. 1(b); in the two cases the exponential growth of the signal-idler pulses sets in at different crystal depths, and they remain temporally locked to the pump pulse until saturation takes place. At saturation, the energy exchange among pump, signal, and idler is strongly reduced, pulses are no more locked and walk each with its own group velocity. The temporal separation between pump and signal at the exit of the crystal depends on the length of this linear propagation regime, and since saturation occurs at randomly varying crystal depths, the signal-pump delay at the end of the crystal shows strong pulse-to-pulse fluctuations. Temporal jitter and energy fluctuation of the pulses are therefore anticorrelated parameters in the OPG process, and will be the two competing aspects that we will take into account in its experimental characterization. Other statistical properties of spectral and temporal parameters of the signal beam are summarized in Table I and exhibit a stable behavior both below and above gain threshold. The stable TL durations and central frequency of the signal demonstrate that the band of the parametric generation process does not fluctuate from pulse to pulse. As observed in previous experiments [3], the pulses are almost TL, confirming the temporal coherence of the OPG pulses, and their duration is about 60% the width of the pump.

According to the field definition given in Eq. (1), the CEP of the signal pulse at generic crystal depth z can be calculated as

$$\phi_1(z) = \phi_L(z) + \phi_{NL}(z), \tag{11}$$

where

$$\phi_L = \omega_1 \tau - k_1 z \tag{12}$$

is the linear phase introduced by the propagation of the carrier field through the crystal and evaluated at the time delay τ when the pulse peak crosses z coordinate, $\phi_{NL} = \angle A_1(z,\tau)$ is an additional phase shift, given by the phase of the complex number $A_1(z,\tau)$, added by the random noise fluctuations and the nonlinear interaction of the three fields.

Figure 3, left panel, shows the values of ϕ_{NL} at $z=z_A$ for the different numerical simulations, and the right panel shows the statistical distribution of ϕ_{NL} both below ($z=z_A$) and above ($z=z_B$) saturation. In both cases ϕ_{NL} exhibits a random uniform distribution between $-\pi$ and π rad; in addition $\phi_{NL}(z_B)$ can be written as

TABLE I. Mean and standard deviation values of the parameters of signal pulses obtained from simulated OPG process. Results are given both below (z_A) and above (z_B) saturation regime.

	$z_A=5$ mm		$z_B=10$ mm	
	μ_A	σ_A	μ_B	σ_B
Energy (μJ)	26.9×10^{-3}	25.46×10^{-3}	3.18	0.032
Signal-pump delay (fs)	7.68	0.66	174.5	14.5
Central frequency (THz)	230.76	0.33	231.35	0.002
TL duration (fs)	33.15	3.55	36.53	0.10
FWHM duration (fs)	39.4	0.18	37.18	0.15

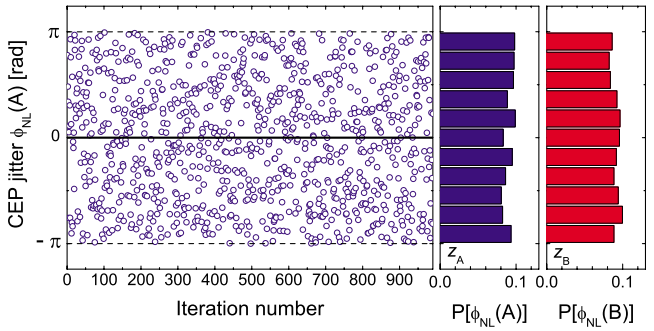

FIG. 3. (Color online) (Left panel) Calculated pulse-to-pulse carrier phase $\phi_{\mathrm{NL}}(z_A)$ of the signal beam; (right panels) statistical distribution of the phase both below (a) and above (b) saturation.

$$\phi_{\mathrm{NL}}(z_B) = \phi_{\mathrm{NL}}(z_A) + \Delta\phi. \tag{13}$$

The phase offset $\Delta\phi$ depends on the longitudinal coordinate in the crystal where the saturation regime sets in; this is an additional nonlinear phase drift that cannot be predicted by those models that neglect pump depletion [48]. If we now consider the linear phase shift ϕ_{L}, we find from Eq. (11) that the generation of phase-stable pulses requires the control not only of the carrier wave, but also of the envelope peak delay τ. In the saturation regime, the signal pulse propagates linearly for a certain crystal length and its CEP slips due to the difference between phase velocity of the pulse carrier and group velocity of the pulse envelope; since the length of this linear propagation undergoes a large fluctuation due to the randomness of the OPG process (see Fig. 2), an additional large fluctuation of the CEP will be introduced. This detrimental effect of time jitter on the CEP suggests that an experimental characterization of the intrinsic CEP of OPG pulses requires operation below the saturation regime.

IV. EXPERIMENTAL SETUP AND RESULTS

The experimental setup used for the investigation of the properties of the OPG pulses driven by a femtosecond laser is shown in Fig. 4. It consists of three parts: (a) a 1-cm-thick BBO crystal for the study of the time jitter of the OPG pulses in the saturation regime; (b) a 3-mm-thick BBO crystal for the investigation of the CEP properties of the OPG pulses below the saturation regime; in this case the OPG pulses are amplified by a two-stage OPA; (c) an f-to-f interferometer for the characterization of CEP and time jitter of the OPG pulses.

A. 1-cm-thick OPG crystal

The results summarized in Table I suggest that pulses generated by a saturated OPG exhibit a significant time jitter due to the quenching of the trapping effect occurring at random positions inside the crystal. In order to experimentally observe this effect and characterize the time jitter, we studied the temporal properties of OPG pulses generated in a 1-cm-thick BBO crystal, according to the setup shown in Fig. 4(a). The OPG is pumped by a regeneratively amplified Ti:sapphire laser, operating at 1 kHz repetition rate and providing

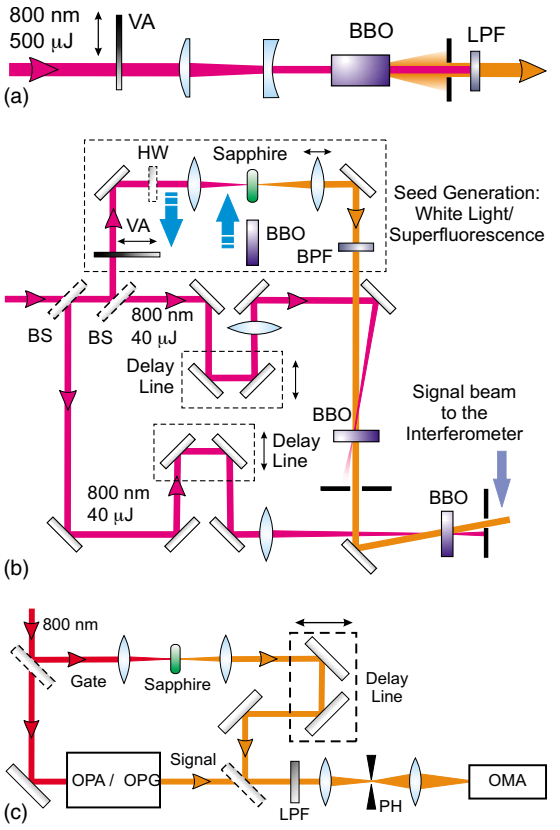

FIG. 4. (Color online) Experimental setup for the characterization of OPG pulses. (a) Single crystal configuration for the study of the temporal jitter of OPG pulses at saturation. LPF, long-pass filter, transmitting $\lambda > 1000$ nm; (b) two-stage OPA for the amplification of a weak signal. The setup can be seeded either by a WLC obtained in a sapphire plate or by OPG from BBO. VA, variable attenuator; HW, half-wave plate; BPF, band-pass filter. (c) f-to-f interferometer to measure the phase and time jitter between signal and gate pulses. PH, 50-μm pin-hole. Pulses under investigation come from either setups (a) or (b).

pulses with 1 mJ energy, 50 fs duration and horizontal polarization at the 800 nm fundamental frequency (FF). A telescope reduces the FF beam diameter to $w = 1.65$ mm, and a variable attenuator controls the pulse power. The crystal is cut at $\theta \approx 26°$ for type II interaction, thus generating an ordinary signal at ~ 1.3 μm and an extraordinary idler at ~ 2.08 μm. Note that in this configuration the signal and the pump have orthogonal polarization, which allowed us to distinguish between the OPG and any parasitic WLC, generated by the pump pulse in the BBO crystal, which would be polarized parallel to the pump. Figure 5 shows an input-output curve of the OPG for pump energy (intensity) up to 430 μJ (200 GW/cm^2), corresponding to the threshold for WLC generation in the BBO crystal. When pumped by 375 μJ the process is at saturation, providing pulses with energy of 13 μJ. The OPG light is emitted over a solid angle around the pump; with the help of an iris, it was possible to select only radiation emitted collinearly to the pump over an angle of 12×10^{-3} sr, corresponding to an energy of 2.3 μJ.

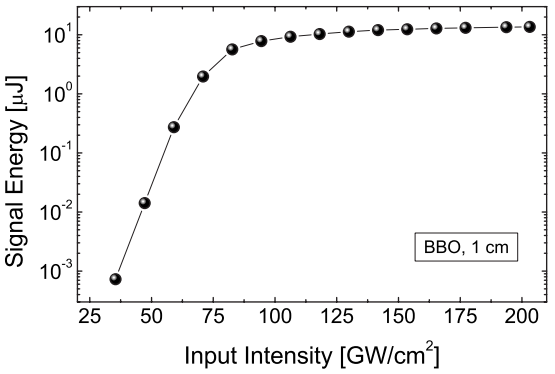

FIG. 5. Input-output curve for the OPG process in the 1-cm-thick BBO crystal.

B. OPG-OPA setup

As discussed above, in order to investigate the CEP preserving properties of the OPG process, we chose to operate below the saturation regime, using a 3-mm-thick BBO crystal. According to the simulations, this allowed us to achieve a nearly constant pump-signal delay, suppressing the jitter-induced CEP fluctuations. As a drawback, the energy of the OPG pulses was too weak and unstable to perform a reliable f-to-f characterization. To overcome this problem, the OPG pulse was amplified by a two-stage FF-pumped OPA, which increased the pulse energy up to the μJ level while preserving the CEP of the signal [49,50].

By focusing a small fraction (10–15 μJ) of the FF pulse energy into the BBO crystal, the OPG pulses are efficiently generated around the pump over a solid angle smaller than 10^{-4} sr. The signal pulses are spectrally selected by a bandpass filter at 1.3 μm and amplified to $\approx$1 μJ in a first stage consisting of a 3-mm-thick BBO crystal, pumped by 40-μJ FF pulses. For this stage we chose a type I configuration since this amplifies only light with ordinary polarization, acting as a filter and rejecting both the spurious WLC generated in the OPG crystal and the extraordinary idler (which would have a different CEP relationship with the pump with respect to the signal). The pulses coming from the first stage are further amplified to $\approx$5 μJ in a second stage, consisting of a 2-mm-thick, type II BBO crystal, pumped by 40 μJ FF pulses. The low pump energy allowed us to operate the second OPA stage close to saturation and to increase the signal energy stability. Even though the absolute phase retrieval from the f-to-f measurement will not be affected by the signal energy fluctuations, a great effort was made to keep them as low as possible, so as to reduce any spurious CEP contribution added after the OPG process.

The seed generation stage of this two-stage OPA setup can be easily modified in order to provide a signal arising from SPM instead of OPG: to this purpose it is sufficient to replace the BBO crystal with a 2-mm thick sapphire plate pumped by a vertically polarized 800 nm beam, thus generating a WLC. If the following amplification stages are maintained unaltered, the change in the seeding stage allows to compare the CEP properties of WLC and OPG; in addition, since SPM preserves the absolute phase of the driving pulse, the measurement of CEP fluctuation of the WLC-seeded OPA allows to evaluate the systematic fluctuations introduced by the two OPA stages and the CEP-characterization system.

C. f-to-f interferometer

For the characterization of CEP fluctuations and time jitter of the signal pulses, we exploited the f-to-f interferometer shown in Fig. 4(c). One arm of the interferometer provided the gate pulse, which was a fraction of the 800 nm FF beam, spectrally broadened by WLC generation in a 3-mm-thick sapphire plate to allow spectral overlap with the signal pulse; the high stability of the laser source guaranteed that the broadened WLC inherited the CEP of the gate pulse, with negligible fluctuations. The signals under investigation, arising either from the OPG or the OPAs, were sent to the second arm of the interferometer; signal and gate were then synchronized by means of a delay line and collinearly combined by a 50:50 beam splitter into an InGaAs spectrometer with single-shot detection capability at 1 kHz. To increase their spatial overlap, we first filtered the two beams by a 50 μm pin-hole [51]; in addition a thin-film polarizer allowed to project the two cross-polarized signal and gate pulses on the same polarization direction and to observe interference fringe patterns. Such patterns provide two different pieces of information: their period is related to the delay between signal and gate, whereas their phase is linked to the CEP phase shift of the signal with respect to the gate. The f-to-f interferometer is therefore not able to provide an absolute measurement of the time delay or the CEP of a pulse train, but just to characterize, on a shot-to-shot basis, the fluctuations of these parameters of the pulse with respect to those of the gate. The described interferometer was therefore used (i) to evaluate the time jitter of the saturated OPG pulses and (ii) to measure the relationship between the CEPs of the signal pulses coming from the OPG/WLC-seeded OPA and the driving pulse at the FF.

D. Results

Figure 6 reports a characterization, obtained with the f-to-f interferometer, of the CEP relationship between the pump and the WLG-seeded OPA. The main panel shows a set of single-shot fringe patterns; the fringe contrast is very high, as shown by the single-shot interferogram reported in the left panel. The measurement shows a remarkably stable fringe pattern: the retrieved pump-signal CEP jitter, given in the upper panel, exhibits a rms of 0.24 rad. This confirms that WLC process maintains the CEP of the pump [26], which is then also preserved in the OPA process [27,49,50]; in addition, these data demonstrate that our measurement system introduces a small amount of spurious fluctuations.

The f-to-f characterization of the OPG-seeded OPA is given in Fig. 7. The main panel shows a series of 1000 single-shot fringe patterns, from which we derived the signal-gate CEP jitter and its statistical distribution given in the upper panels. The measurement shows an absolute phase with a uniform distribution $P(\phi)$ in the $(-\pi,\pi)$ range, thus confirming that the OPG process is not able to preserve the CEP of the pump pulses. This result clearly indicates that in

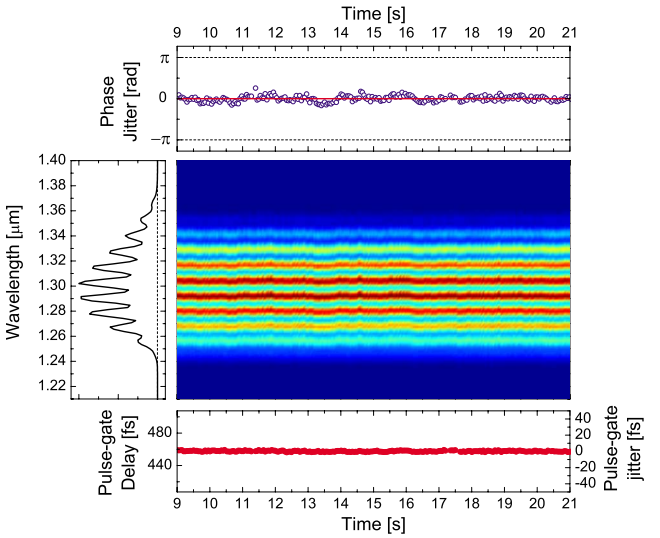

FIG. 6. (Color online) f-to-f single-shot interferometric trace of the amplified WLC. Upper panel: retrieved signal-gate phase jitter. Lower panel: retrieved pulse-gate delay and jitter. Temporal jitter exhibits fluctuations with rms $\sigma \approx 1$ fs.

an OPA, when the seed pulse is generated by the OPG process, the idler self-phase-stabilization mechanism does not work. The interferograms also allow measuring the time jitter occurring between the amplified signal and the gate; both the WLC- and the OPG-seeded OPA pulses exhibit a low jitter (lower panels of Figs. 6 and 7, respectively), confirming that they are substantially temporally locked with the pump pulses.

The characterization of the timing jitter of the OPG pulses under pump depletion conditions was performed using the 1-cm-thick BBO crystal. The measurement was performed evaluating only the collinear radiation from the OPG process

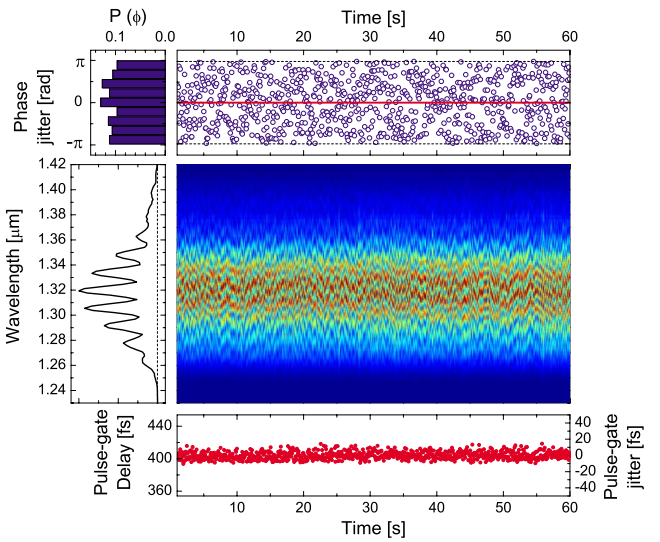

FIG. 7. (Color online) f-to-f single-shot interferometric trace of the amplified OPG pulse. Upper panel: retrieved signal-gate phase jitter, together with its statistical distribution $P(\varphi)$. Lower panel: retrieved pulse-gate delay and jitter (same scale as in Fig. 6). Temporal jitter exhibits fluctuations with rms $\sigma \approx 4.5$ fs.

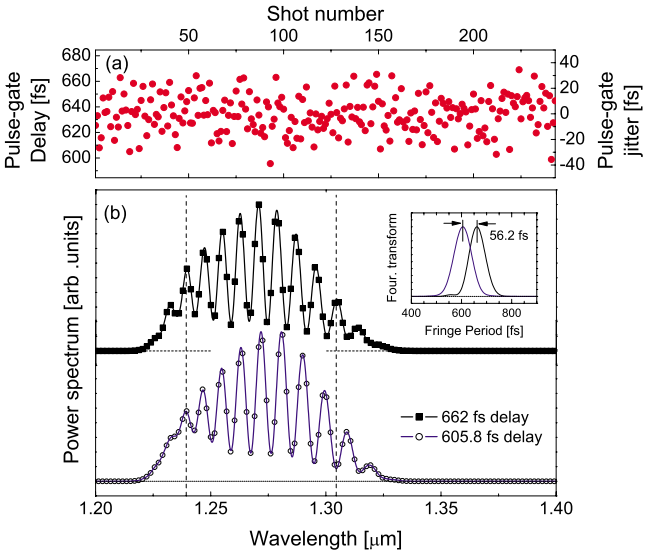

FIG. 8. (Color online) f-to-f single-shot interferometric measurement of OPG from the 1 cm BBO. (a) Retrieved pulse-gate delay and jitter, displayed in the same scale as Figs. 6 and 7. (b) Fringe patterns selected from the same measurement run, showing different periods due to a jitter in the delay of the emitted OPG pulse; points: measurement; solid line: interpolation. Inset: Fourier transforms of the fringes.

selected by the iris. The recorded f-to-f interferogram reveals a very strong time jitter demonstrated by a change in the fringe period; Fig. 8(a) shows the jitter for 250 consecutive shots, displaying an rms fluctuation of 14.2 fs, in excellent agreement with the simulated value reported in Table I. Figure 8(b) reports two of such fringe patterns, characterized by different periods; the inset shows their intensity Fourier transforms, and confirms that the two corresponding signal pulses are emitted with different delays from the OPG crystal. In particular, the reported measurement corresponds to a fluctuation of ≈ 56 fs, which is larger than the expected OPG pulse duration of ≈ 36 fs.

V. CONCLUSION

In this paper we have investigated, both numerically and experimentally, the OPG process driven by femtosecond pulses, focusing on parameters such as CEP and time jitter. By solving numerically the coupled second-order three-wave nonlinear propagation equations in the plane-wave limit, using noise fields to mimic the vacuum fluctuations, we found that there is no correlation between the CEPs of the OPG pulse and the pump pulse; in addition, when the OPG process is driven into saturation, the generated pulses exhibit a strong temporal jitter with respect to the driving pulses.

Experimentally, we have characterized the OPG process in a BBO crystal driven by 50 fs pulses at 800 nm. For an OPG in the saturation regime, we have evidenced a timing jitter with respect to the pump pulses, which may become important in some experiments, such as pump-probe, especially with short driving pulses. We have also studied with an f-to-f interferometer the CEP relationship between pump and

signal in an OPA, seeded by either OPG or WLC. We found that, while the WLC-seeded OPA preserves the CEP of the pump, this relationship is completely lost in the case of OPG seed. These results indicate that OPG-seeded OPAs cannot be used in passive CEP stabilization schemes.

ACKNOWLEDGMENT

This work was partially supported by the European Union within Contract No. RII3-CT-2003-506350 (Laserlab Europe).

[1] *Ultrafast Phenomena XV*, Springer Verlag Series in Chemical Physics Vol. 88, edited by P. Corkum, D. Jonas, D. Miller, and A. M. Weiner (Springer-Verlag, Berlin, 2007).
[2] R. Boyd, *Nonlinear Optics*, 3rd ed. (Academic, New York, 2008).
[3] V. V. Yakovlev, B. Kohler, and K. R. Wilson, Opt. Lett. **19**, 2000 (1994).
[4] M. Nisoli, S. Stagira, S. De Silvestri, O. Svelto, G. Valiulis, and A. Varanavicius, Opt. Lett. **23**, 630 (1998).
[5] *The Supercontinuum Laser Source*, edited by R. R. Alfano (Springer, New York, 1989).
[6] A. L. Gaeta, Phys. Rev. Lett. **84**, 3582 (2000).
[7] S. E. Harris, M. K. Oshman, and R. L. Byer, Phys. Rev. Lett. **18**, 732 (1967).
[8] G. P. Banfi, R. Danielius, A. Piskarskas, P. Di Trapani, P. Foggi, and R. Righini, Opt. Lett. **18**, 1633 (1993).
[9] F. Seifert, V. Petrov, and F. Noack, Opt. Lett. **19**, 837 (1994).
[10] C. Schriever, S. Lochbrunner, P. Krok, and E. Riedle, Opt. Lett. **33**, 192 (2008).
[11] A. Galvanauskas, M. A. Arbore, M. M. Fejer, M. E. Fermann, and D. Harter, Opt. Lett. **22**, 105 (1997).
[12] T. Südmeyer, J. Aus der Au, R. Paschotta, U. Keller, P. G. R. Smith, G. W. Ross, and D. C. Hanna, J. Phys. D **34**, 2433 (2001).
[13] F. Brunner, E. Innerhofer, S. V. Marchese, T. Südmeyer, R. Paschotta, T. Usami, H. Ito, S. Kurimura, K. Kitamura, G. Arisholm, and U. Keller, Opt. Lett. **29**, 1921 (2004).
[14] X. Xie, A. M. Schober, C. Langrock, R. V. Roussev, J. R. Kurz, and M. M. Fejer, J. Opt. Soc. Am. B **21**, 1397 (2004).
[15] S. V. Marchese, E. Innerhofer, R. Paschotta, S. Kurimura, K. Kitamura, G. Arisholm, and U. Keller, Appl. Phys. B: Lasers Opt. **81**, 1049 (2005).
[16] M. Tiihonen, V. Pasiskevicius, A. Fragemann, C. Canalias, and F. Laurell, Appl. Phys. B: Lasers Opt. **85**, 73 (2006).
[17] P. S. Kuo, K. L. Vodopyanov, M. M. Fejer, D. M. Simanovskii, X. Yu, J. S. Harris, D. Bliss, and D. Weyburne, Opt. Lett. **31**, 71 (2006).
[18] A. Baltuška, M. Uiberacker, E. Goulielmakis, R. Keinberger, V. S. Yakovlev, T. Udem, T. W. Hänsch, and F. Krausz, IEEE J. Sel. Top. Quantum Electron. **9**, 972 (2003).
[19] G. G. Paulus, F. Grabson, H. Walther, P. Villoresi, M. Nisoli, S. Stagira, E. Priori, and S. De Silvestri, Nature (London) **414**, 182 (2001).
[20] A. Baltuška, T. Udem, M. Uiberacker, M. Hentschel, E. Goulielmakis, C. Gohle, R. Holzwarth, V. S. Yakovlev, A. Scrinzi, T. W. Hänsch, and F. Krausz, Nature (London) **421**, 611 (2003).
[21] R. Kienberger, E. Goulielmakis, M. Uiberacker, A. Baltuška, V. Yakovlev, F. Bammer, A. Scrinzi, Th. Westerwalbesloh, U. Kleineberg, U. Heinzmann, M. Drescher, and F. Krausz, Nature (London) **427**, 817 (2004).
[22] G. Sansone, E. Benedetti, F. Calegari, C. Vozzi, L. Avaldi, R. Flammini, L. Poletto, P. Villoresi, C. Altucci, R. Velotta, S. Stagira, S. De Silvestri, and M. Nisoli, Science **314**, 443 (2006).
[23] S. T. Cundiff and J. Ye, Rev. Mod. Phys. **75**, 325 (2003).
[24] A. Baltuška, T. Fuji, and T. Kobayashi, Phys. Rev. Lett. **88**, 133901 (2002).
[25] G. Cerullo and S. De Silvestri, Rev. Sci. Instrum. **74**, 1 (2003).
[26] M. Bellini and T. W. Hänsch, Opt. Lett. **25**, 1049 (2000).
[27] P. Baum, S. Lochbrunner, J. Piel, and E. Riedle, Opt. Lett. **28**, 185 (2003).
[28] P. Baum, E. Riedle, M. Greve, and H. R. Telle, Opt. Lett. **30**, 2028 (2005).
[29] X. Fang and T. Kobayashi, Opt. Lett. **29**, 1282 (2004).
[30] S. Adachi, P. Kumbhakar, and T. Kobayashi, Opt. Lett. **29**, 1150 (2004).
[31] C. Manzoni, D. Polli, G. Cirmi, D. Brida, S. De Silvestri, and G. Cerullo, Appl. Phys. Lett. **90**, 171111 (2007).
[32] M. Kakehata, H. Takada, Y. Kobayashi, K. Torizuka, Y. Fujihara, T. Homma, and H. Takahashi, Opt. Lett. **26**, 1436 (2001).
[33] C. P. Hauri, R. B. Lopez-Martens, C. I. Blaga, K. D. Schultz, J. Cryan, R. Chirla, P. Colosimo, G. Doumy, A. M. March, C. Roedig, E. Sistrunk, J. Tate, J. Wheeler, L. F. DiMauro, and E. P. Power, Opt. Lett. **32**, 868 (2007).
[34] W. H. Louisell, A. Yariv, and A. E. Siegman, Phys. Rev. **124**, 1646 (1961).
[35] G. Arisholm, J. Opt. Soc. Am. B **16**, 117 (1999).
[36] A. Fix and R. Wallenstein, J. Opt. Soc. Am. B **13**, 2484 (1996).
[37] D. A. Kleinman, Phys. Rev. **174**, 1027 (1968).
[38] Y. Guan, J. W. Haus, and P. Powers, Phys. Rev. A **71**, 023809 (2005).
[39] E. Sidick, A. Knoesen, and A. Dienes, J. Opt. Soc. Am. B **12**, 1704 (1995).
[40] S. A. Akhmanov, V. A. Vysloukh, and A. S. Chirkin, *Optics of Femtosecond Laser Pulses* (American Institute of Physics, New York, 1992).
[41] G. Cirmi, C. Manzoni, D. Brida, S. De Silvestri, and G. Cerullo, J. Opt. Soc. Am. B **25**, B62 (2008).
[42] G. P. Agrawal, *Nonlinear Fiber Optics*, 3rd ed. (Academic, Boston, 2001).
[43] A. Picozzi and M. Haelterman, Phys. Rev. E **63**, 056611 (2001).
[44] F. Haake, H. King, G. Schröder, J. Haus, R. Glauber, and F. Hopf, Phys. Rev. Lett. **42**, 1740 (1979).
[45] R. Danielius, A. Piskarskas, A. Stabinis, G. P. Banfi, P. Di Trapani, and R. Righini, J. Opt. Soc. Am. B **10**, 2222 (1993).
[46] G. Marsaglia and A. Zaman, Ann. Appl. Probab. **1**, 462

(1991).
[47] R. L. Byer and S. E. Harris, Phys. Rev. **168**, 1064 (1968).
[48] I. N. Ross, P. Matousek, G. H. C. New, and K. Osvay, J. Opt. Soc. Am. B **19**, 2945 (2002).
[49] C. Hauri, P. Schlup, G. Arisholm, J. Biegert, and U. Keller, Opt. Lett. **29**, 1369 (2004).
[50] R. Zinkstok, S. Witte, W. Hogervorst, and K. Eikema, Opt. Lett. **30**, 78 (2005).
[51] A. Baltuška, T. Fuji, and T. Kobayashi, Opt. Lett. **27**, 1241 (2002).